Magnetic field properties in a birdcage coil

Patrice Boissoles, Gabriel Caloz

Magnetic field properties in a birdcage coil

P. Boissoles and G. Caloz

March 15, 2006

Abstract

Radiofrequency magnetic fields used in MRI experiments have to satisfy specific properties. First, they need to be as homogeneous as possible to excite uniformly the nuclei. Secondly, as the nuclei, these fields need to have a precession movement at Larmor frequency. In this paper we present a numerical study of these properties in the case of the birdcage coil. We derive analytic expression of the RF field through an equivalent circuit model. Properties are validated through numerical simulations.

1 Introduction

Since their introduction over two decades ago, birdcage coils ([1, 2, 3]) are often used in MRI experiments because they generate an adequate homogeneous radiofrequency magnetic field. Since then several studies have used the equivalent circuit method to predict first the mutual inductances between conductors and then the resonant spectrum. Hayes et al. ([1]) showed that a N leg coil has $N/2+1$ different resonant modes but neither gave the expression of the magnetic field generated not got numerical simulations. Leifer ([4]) showed that another resonant mode, called the Helmholtz mode, exists. Since then, there is an agreement about the $N/2+2$ analytic formulas of the resonant frequencies of a N leg coil in function of the mutual inductance and the capacitance.

Analytic expressions of the radiofrequency magnetic field and numerical simulations can be found in [5] and [6]. These results concerned only the magnetic field associated to the first resonant mode and its homogeneity. In [7] we can find a brief homogeneity analysis with respect to the resonant frequency but no information on the simulations. Let us mention other models based on the Time-Domain Finite-Difference method ([8]) to calculate the radiofrequency field generated by the coil. Of course papers using this technique do not give analytic formulas. Moreover with this approach we can only handle rough approximations of the magnetic field since we need to use a three-dimensional structured mesh of the antenna.

In our paper, we are introducing a model close to the ones of [1] and [6]. We add the electrical resistance of the conductors and the tension sources. By using the classical electrical network theory we get the same formulas for the resonant frequencies as in [4] and an analytic expression of the magnetic field associated. We study the homogeneity and the precession movement of the magnetic fields associated to the different resonant frequencies through numerical simulations.

More precisely the content and the organisation of the paper are the following. In section 2 we briefly present the circuit analysis of the birdcage coil and give the expression of the different radiofrequency magnetic fields associated to each resonant frequency. In section 3 the algorithm used to do the simulations is briefly presented. In particular we explain the validation procedure. Section 4 is devoted to the two particular pulsations ω_{AR} and ω_{CR}. We explain why these pulsations are not appropriate for applications in MRI. In section 5 we study the homogeneity of the magnetic field with respect to the frequency and to the number N of legs. Through numerical simulations we show how the mode 1 is the only appropriate one for applications in MRI. Finally section 6 is devoted to the precession movement of magnetic field associated to the mode 1. In particular, we study the deviation to the circular movement when we move inside the birdcage coil.

2 Birdcage coil circuit analysis

We consider a N leg bandpass birdcage coil with capacitors in both endrings and legs (see Fig. 1).

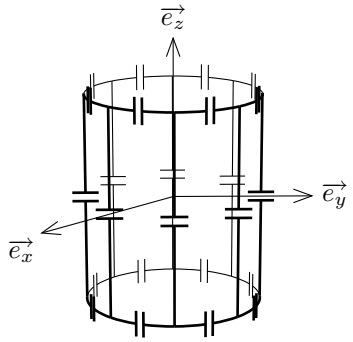

Figure 1: Bandpass birdcage coil

Our electric equivalent circuit is based on electrical network theory. We model each conductor as an inductance and a resistance. Thus the bandpass birdcage coil is described as the repetition of the electric network segment shown in Fig. 2, with left and right-most ends connected together.

In Fig. 2, L^{b} represents the self-inductance of a single leg, L^{a} the self-inductance of a single endring arc, C^{a} the capacitance of the capacitor between two legs and C^{b} represents the capacitance of the capacitor between two opposite endring arcs. This model includes the lowpass and highpass coils as special cases when $1/C^{\mathrm{a}}$ or $1/C^{\mathrm{b}}$ is set to zero.

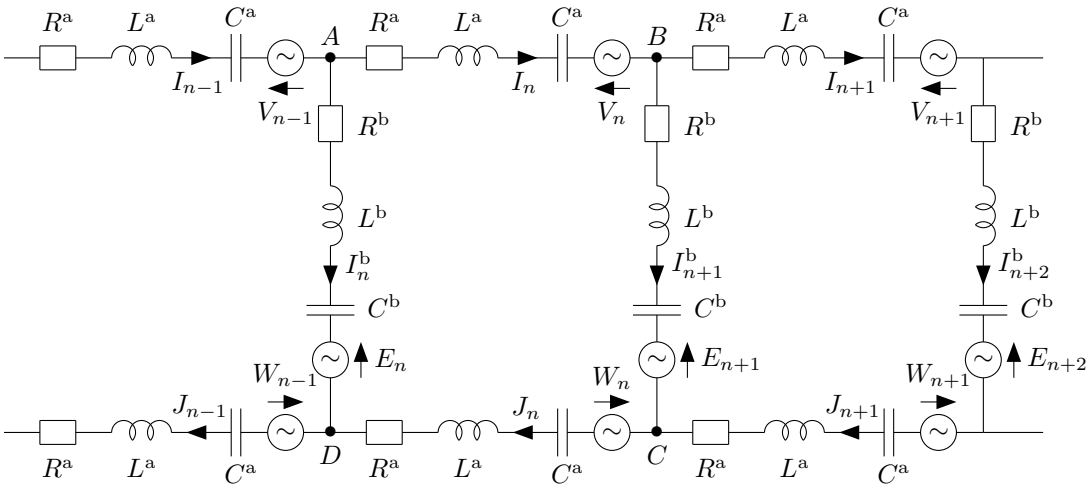

Figure 2: A section of the birdcage equivalent circuit

By applying the Kirchhoff law, we can derive the general system of equations satisfied by the current of the endrings. In the configurations used in practice, we show in [9] and [11] that we can solve explicitly this system and give the expression of the $N/2+2$ resonance pulsations: ω_{AR}, ω_1, ..., ω_{N-1}, and ω_{CR}. The two modes associated to ω_{AR} and ω_{CR} differ from the others. Indeed equal currents flow in each end ring and do not produce a transverse magnetic field in the sample region. These modes are called the anti-rotating (AR) and the co-rotating (CR) ring modes. The resonant pulsations satisfy the symmetry relation (see [1, 4]):

$$\forall\, 1 \leqslant k \leqslant N,\ \omega_{N-k} = \omega_k. \tag{1}$$

So in the next sections we will only study the radiofrequency magnetic field associated to the pulsations ω_{AR}, ω_{CR} and ω_k, $1 \leqslant k \leqslant N/2$.

The expression of the radiofrequency field associated to the pulsation ω_k (also called the mode k) outside the conductors is given by the Biot-Savart formula:

$$\begin{aligned} B_k \;=\; & \frac{\mu_0 I_0}{4\pi} \sum_{j=1}^{N} \left[\int_{\theta_j}^{\theta_{j+1}} \frac{d\theta}{[a^2(\theta, L/2)]^{3/2}} \begin{pmatrix} (z-L/2)\, R\cos\theta \\ (z-L/2)\, R\sin\theta \\ (-y\sin\theta - x\cos\theta + R)\, R \end{pmatrix} \right. \\ & - \int_{\theta_j}^{\theta_{j+1}} \frac{d\theta}{[a^2(\theta, -L/2)]^{3/2}} \begin{pmatrix} (z+L/2)\, R\cos\theta \\ (z+L/2)\, R\sin\theta \\ (-y\sin\theta - x\cos\theta + R)\, R \end{pmatrix} \\ & + 2i \exp\left(-\frac{ik\pi}{N}\right) \sin\left(\frac{k\pi}{N}\right) \frac{1}{(x - R\cos\theta_j)^2 + (y - R\sin\theta_j)^2} \\ & \times \left. \begin{pmatrix} (y - R\sin\theta_j) \left(\frac{z-L/2}{\sqrt{a^2(\theta_j, L/2)}} - \frac{z+L/2}{\sqrt{a^2(\theta_j, -L/2)}} \right) \\ -(x - R\cos\theta_j) \left(\frac{z-L/2}{\sqrt{a^2(\theta_j, L/2)}} - \frac{z+L/2}{\sqrt{a^2(\theta_j, -L/2)}} \right) \\ 0 \end{pmatrix} \right] \exp(ik\theta_j) \end{aligned} \tag{2}$$

where θ_j and $a^2(\theta, Z)$ are given by:

$$\begin{cases} \theta_j = \dfrac{2\pi(j-1)}{N}, \\ a^2(\theta, Z) = (x - R\cos\theta)^2 + (y - R\sin\theta)^2 + (z - Z)^2. \end{cases} \tag{3}$$

The expression of the field associated to ω_{AR} is obtained by setting $k = 0$ in eq 2. The one of the field associated to ω_{CR} is obtained by setting $k = 0$ in eq 2 and by changing the minus before the second integral in a plus.

3 Numerical method

From the birdcage coil circuit analysis presented in section 2 we have written a Matlab program to calculate the different resonant pulsations and the radiofrequency field associated.

As mentionned in the introduction the formula of the resonant pulsations involves the mutual inductance between conductors. In particular we need to know with accuracy the shape of the leg and the ring. To compute the mutual inductances we use the method detailed in [11]. We have validated the method through numerical simulations which were compared to experimental results.

As we can see from eq 2 the part of the program devoted to the radiofrequency field needs only the value of k, N, L, R, and the coordinates (x, y, z). To efficiently compute the magnetic field we have developed the different integrals in eq 2 using the elliptic integrals (see [10]). A detailed analysis is given in [9]. This part of our program has been validated by comparison to analytic results in the case of isolated leg and ring. Moreover we have checked that the calculated field satisfies the equations

$$\operatorname{div} B_k = 0, \ \operatorname{rot} B_k = 0, \tag{4}$$

which are consequences of the Biot-Savart formula. Here div and rot denote the classical divergence and rotational differential operators.

The characteristics of the lowpass birdcage coil used for the results presented here are:

$$\begin{cases} L = 12.8 \text{ cm}, \ R = 4.45 \text{ cm}, \ N = 16, \\ C^{\mathrm{a}} = 180 \text{ pF}, \ C^{\mathrm{b}} = 0 \text{ pF}. \end{cases} \tag{5}$$

4 Pulsations $\omega_{\mathbf{AR}}$ and $\omega_{\mathbf{CR}}$

For the pulsations ω_{AR} and ω_{CR} an equal current is flowing in each end ring and no current in the legs of the coil. Thus the homogeneity of the magnetic fields associated to these pulsations does not depend of N, the number of leg.

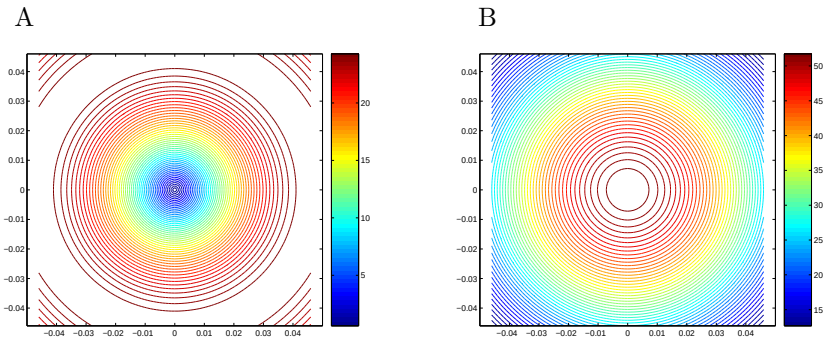

Figure 3: Norm of B_{AR} (a) and B_{CR} (b) field

We note B_{AR} the field associated to the pulsation ω_{AR} and B_{CR} the one associated to ω_{CR}. To study the homogeneity of these fields, we plot in Fig. 3

their Euclidean vector norm in the plane perpendicular to the birdcage axis in its middle. We can see that their norm is a function of the radius, that is they are not homogeneous at all. These two magnetic fields are not appropriate for applications in MRI, where we need a constant field in the center of the antenna.

5 Homogeneity

5.1 Homogeneity with respect to k

To discuss the homogeneity of the field B_k with respect to k we plot in Fig. 4 the magnetic field patterns in the plane perpendicular to the birdcage axis in its middle for k between 1 and $8 = N/2$. To compare the different fields we have normalized them.

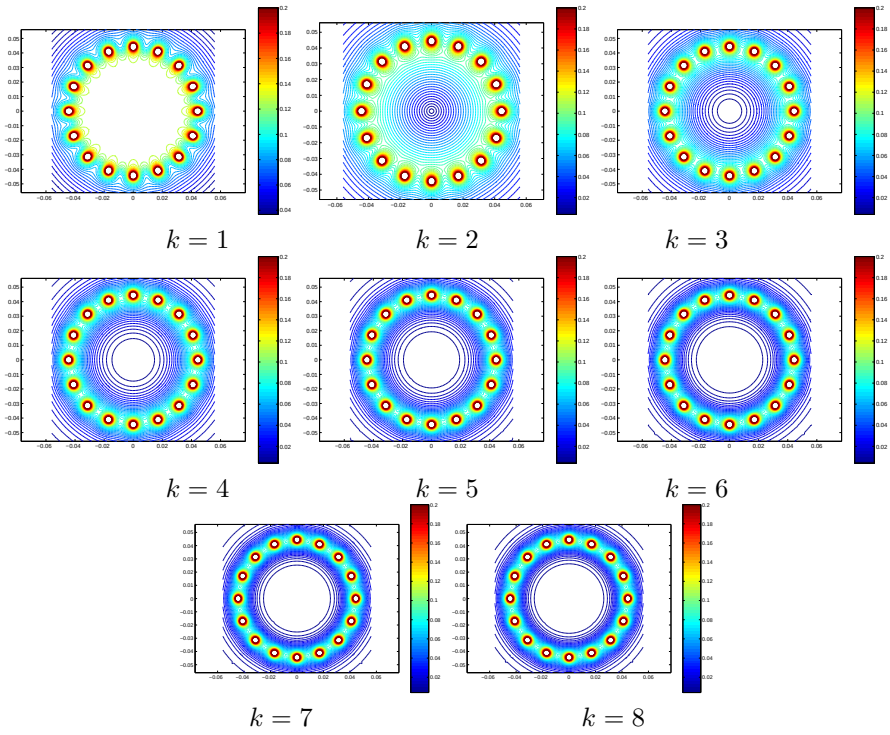

Figure 4: Norm of B_k field for different modes k

We see that the first mode is the only one for which the field is homogeneous in the central area. In order to verify the magnetic field homogeneity and to justify the choice of the mode 1 in MRI, we plot the mode k field along the y axis for k between 1 and 8 on Fig. 5. We remark that only the field associated to the mode 1 is not zero at the center of the birdcage coil. It is the only one

with energy and homogeneity property in the center. That is why it is precisely the one used in MRI.

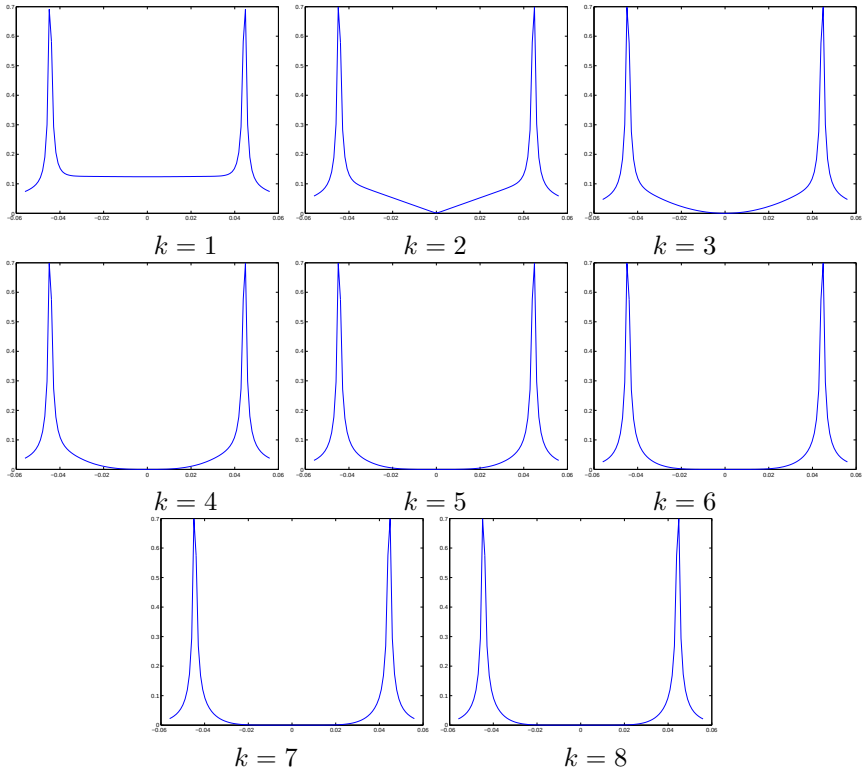

Figure 5: Norm of B_k field for different modes k

Now we will study homogeneity of the B_1 field along the z axis. For this, we plot on Fig. 6.a the magnetic field pattern for the mode 1 in the plane of

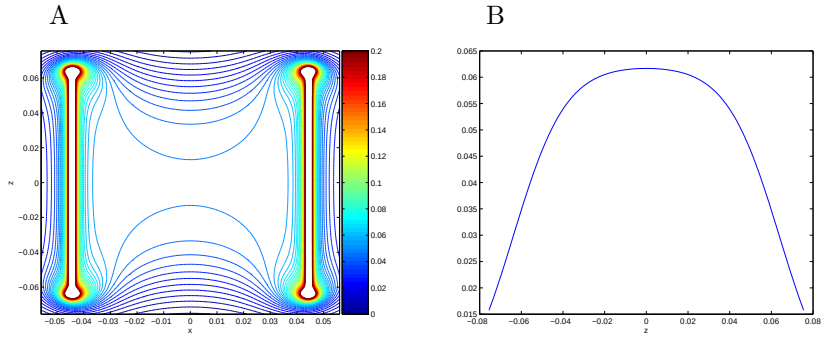

Figure 6: Norm of B_1 field in the plane xz (a) and along the z axis (b)

equation $y = 0$ containing the birdcage axis. As mentioned in the literature we verify that the field is still homogeneous at the center of the birdcage coil. More precisely, Fig. 6.b shows that in the area defined by a z coordinate between $-L/8 = -0.016$ cm and $L/8$ the mode 1 field is homogeneous.

5.2 Homogeneity with respect to N

Since we know that the B_1 field is the most homogeneous one, we will study how this homogeneity varies with respect to N, the number of legs. For this, we plot on Fig. 7 the magnetic field pattern in the plane perpendicular to the birdcage axis in its middle for N between 2 and 12. The more legs the coil has, the more homogeneous the field is.

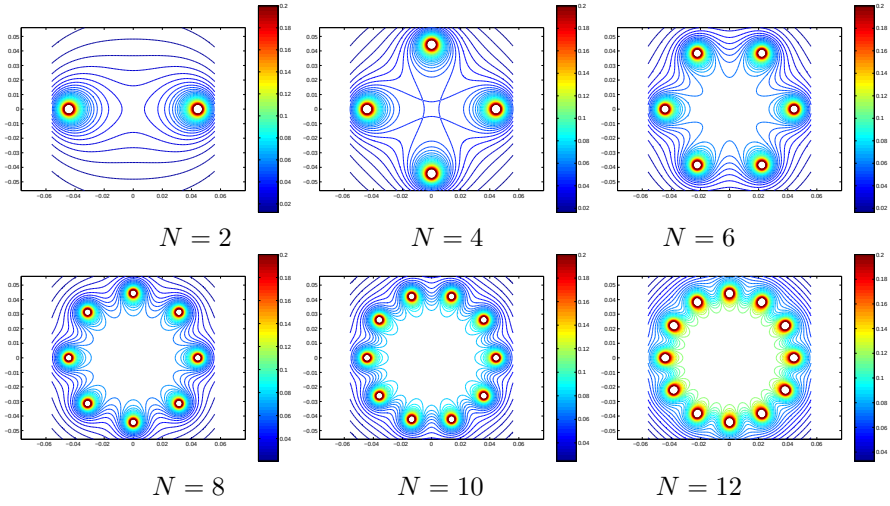

Figure 7: Norm of B_1 field for different values of N

6 Precession movement

This section is devoted to the study of the precession movement of the B_1 field. For this we consider the real field, that is $\Re\left(B_k e^{-i\omega_1 t}\right)$ and not the complex one anymore. First, in Fig. 8 we start at the center of the coil: $(x, y, z) = (0, 0, 0)$. The different diagrams show that the B_1 field has a circular movement at the center of the coil. Moreover we see that the trajectory of B_1 moves in the xy plane, thus B_1 is orthogonal to the birdcage axis, which is an important property too.

In Fig. 9 to Fig. 12, along the x axis we consider successively $x = R/4$, $x = R/2$, $x = 3R/4$, and $x = 9R/10$. For each point we plot a $3D$ view of the movement, the projection in the xy plane, and the L^2 norm. The first third

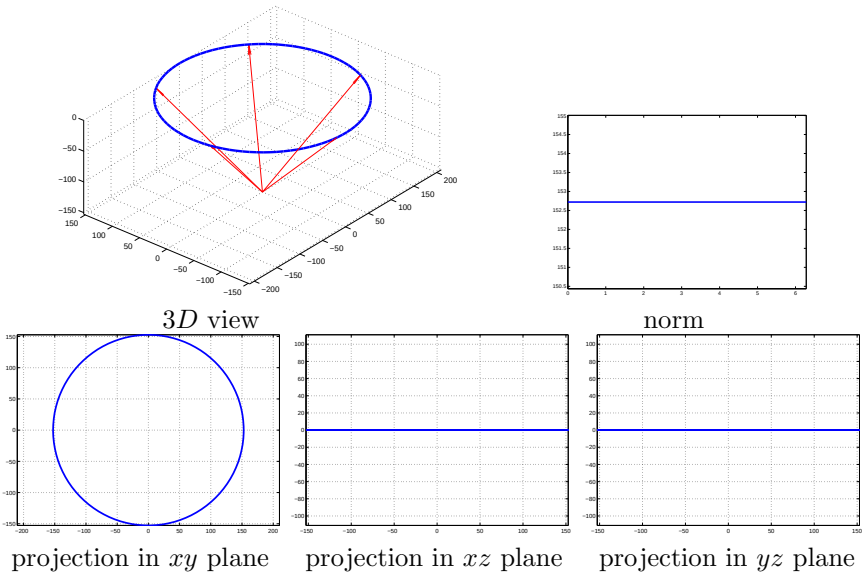

Figure 8: Trajectory of B_1 field at point $(0, 0, 0)$

cases are very close to the circular movement as shown by the table 1. Moreover as in the first case we can show that the trajectory of B_1 remains orthogonal to the birdcage axis. In MRI experiments the static field used is parallel to the birdcage axis so these simulations ensured that the radiofrequency field is perfectly orthogonal to the static field along the x axis.

Coordinate	Major axis	Minor axis	Relative quotient
$(0, 0, 0)$	152,7210	152,7210	0,0000 %
$(R/4, 0, 0)$	153,2308	153,0630	0,1095 %
$(R/2, 0, 0)$	154,3967	153,8768	0,3367 %
$(3R/4, 0, 0)$	157,8201	156,0395	1,1282 %
$(9R/10, 0, 0)$	225,4329	190,6530	15,4280 %

Table 1: Variation of the major and minor axis with respect to x

In the last figure, the major and minor axis at the point $(0, 0, 9R/10)$ are very different and the movement is not close to a circle at all. We observe the same relative quotients when moving along the y axis. We can prove that the relative quotient is less than 1 when moving along the z axis for z between $-3L/8$ and $3L/8$. In conclusion, in a cylinder with a radius of $3R/4$ and height of $3L/4$, the B_1 field has a movement close to the circular one, up to 1%.

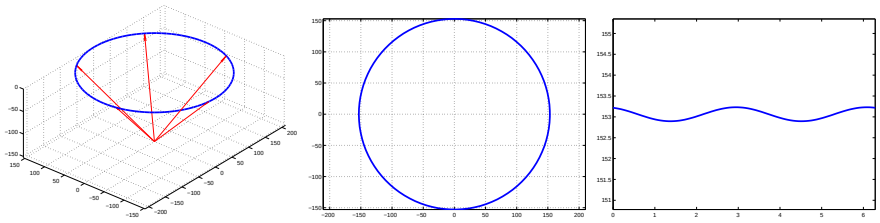

$3D$ view projection in xy plane norm

Figure 9: Trajectory of B_1 field at point $(R/4, 0, 0)$

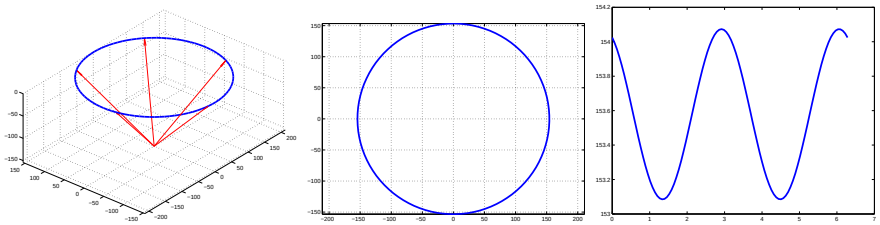

$3D$ view projection in xy plane norm

Figure 10: Trajectory of B_1 field at point $(R/2, 0, 0)$

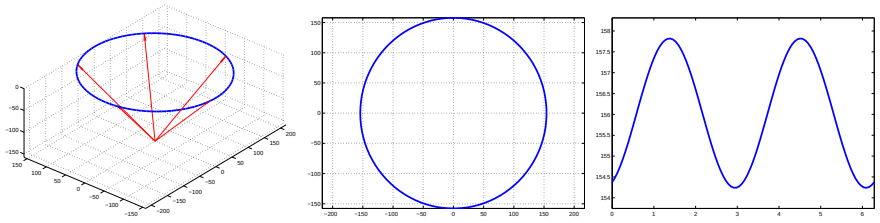

$3D$ view projection in xy plane norm

Figure 11: Trajectory of B_1 field at point $(3R/4, 0, 0)$

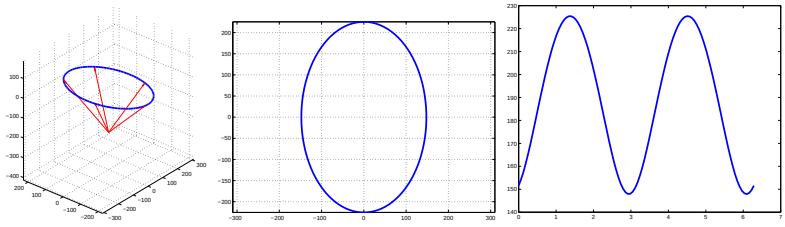

$3D$ view projection in xy plane norm

Figure 12: Trajectory of B_1 field at point $(9R/10, 0, 0)$

7 Conclusion

In this paper we have presented a numerical study of the main properties that the radiofrequency magnetic field should have in MRI experiments. We have shown why the mode 1 is the only one suitable in MRI. In particular we have justified the usual assumption of circular movement found in the literature. We also have presented a study of homogeneity for the radiofrequency field associated to the first mode with respect to the number of legs. A mathematical analysis of these properties and much more theorical developments can be found in [9].

Let us mention that the method and the algorithm described in this paper can be used to study the properties of any other birdcage coil without modifications. It will be interesting to adapt our method to study other MRI antenna.

References

[1] Hayes C, Edelstein W, Schenck J, Mueller O, Eash M. An efficient, highly homogeneous radiofrequency coil for whole-body nmr imaging at 1.5 T. J Magn Reson 1985;63:622–628.

[2] Tropp J. The theory of the bird-cage resonator. J Magn Reson 1989;82:51–62.

[3] Tropp J. Mutual inductance in the bird-cage resonator. J Magn Reson 1997;126:9–17.

[4] Leifer MC. Resonant modes of the birdcage coil. J Magn Reson 1997;124:51–60.

[5] Li S, Collins CM, Dardzinski BJ, Chin C, Smith MB. A method to create an optimum current distribution and homogeneous B_1 field for elliptical birdcage coils. Magn Reson Med 1997;37:600–608.

[6] Doty FD, Entzminger GJ, Hauck CD, Staab JP. Practical aspects of birdcage coils. J Magn Reson 1999;138:144–154.

[7] Giovannetti G, Landini L, Santarelli MF, Positano F. A fast and accurate simulator for the design of birdcage coils in mri. MAGMA 2002;15:36–44.

[8] Lau RWM, Sheppard RJ. The modelling of biological systems in three dimensions using the time domain finite-difference method : I. the implementation of the model. Phys Med Biol 1986;31:1247–1256.

[9] Boissoles P. Problèmes mathématiques et numériques issus de l'imagerie par résonance magnétique nucléaire [thèse]. Rennes : université de Rennes 1 ; 2005. p. 1–274.

[10] Chu Y. Numerical calculation for the magnetic field in current-carrying circular arc filament. IEEE Transactions on magnetics (1998);34:502–504.

[11] Boissoles P, Caloz G. Accurate calculation of mutual inductance and magnetic fields in a birdcage coil. Preprint IRMAR 2006;06-07.